Van der Waals Epitaxial Growth of Two-Dimensional Single-Crystalline GaSe Domains on Graphene

Xufan Li,[†] Leonardo Basile,[†,‡] Bing Huang,[†] Cheng Ma,[†] Jaekwang Lee,[†] Ivan V. Vlassiouk,[§] Alexander A. Puretzky,[†] Ming-Wei Lin,[†] Mina Yoon,[†] Miaofang Chi,[†] Juan C. Idrobo,[†] Christopher M. Rouleau,[†] Bobby G. Sumpter,[†,#] David B. Geohegan,[†] and Kai Xiao*[,†]

[†]Center for Nanophase Materials Sciences, Oak Ridge National Laboratory, Oak Ridge, Tennessee 37831, United States, [‡]Departamento de Física, Escuela Politécnica Nacional, Quito 170525, Ecuador, [#]Computer Science and Mathematics Division, Oak Ridge National Laboratory, Oak Ridge, Tennessee 37831, United States, and [§]Energy & Transportation Science Division, Oak Ridge National Laboratory, Oak Ridge, Tennessee 37831, United States

ABSTRACT Two-dimensional (2D) van der Waals (vdW) heterostructures are a family of artificially structured materials that promise tunable optoelectronic properties for devices with enhanced functionalities. Compared to transferring, direct epitaxy of vdW heterostructures is ideal for clean interlayer interfaces and scalable device fabrication. Here we report the synthesis and preferred orientations of 2D GaSe atomic layers on graphene (Gr) by vdW epitaxy. GaSe crystals are found to nucleate predominantly on random wrinkles or grain boundaries of graphene, share a preferred lattice orientation with underlying graphene, and grow into large (tens of micrometers) irregularly shaped, single-crystalline domains. The domains are found to propagate with triangular edges that merge into the large single crystals during growth. Electron diffraction reveals that approximately 50% of the GaSe domains are oriented with a 10.5 ± 0.3° interlayer rotation with respect to the underlying graphene. Theoretical investigations of interlayer energetics reveal that a 10.9° interlayer rotation is the most energetically preferred vdW heterostructure. In addition, strong charge transfer in these GaSe/Gr vdW heterostructures is predicted, which agrees with the observed enhancement in the Raman E^2_{1g} band of monolayer GaSe and highly quenched photoluminescence compared to GaSe/SiO_2. Despite the very large lattice mismatch of GaSe/Gr through vdW epitaxy, the predominant orientation control and convergent formation of large single-crystal flakes demonstrated here is promising for the scalable synthesis of large-area vdW heterostructures for the development of new optical and optoelectronic devices.

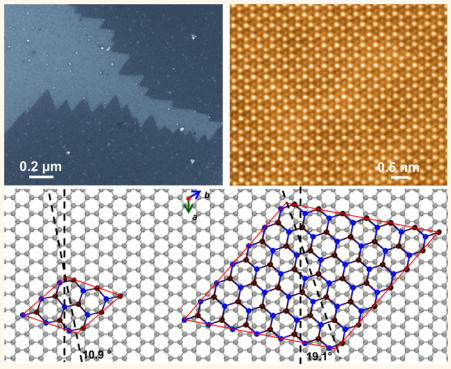

KEYWORDS: van der Waals epitaxy · heterostructures · GaSe · chemical vapor deposition · graphene

Given the variety of optical and electronic properties of two-dimensional (2D) layered materials including metallic graphene, insulating hexagonal boron nitride (*h*BN), and semiconducting metal mono- and dichalcogenides with different band gaps, the heterogeneous engineering of 2D crystals provides exciting opportunities to create novel properties and devices with enhanced functionalities.[1−10] One promising type of heterostructures with atomically sharp interfaces can be realized by vertically stacking 2D layers that are held together by van der Waals (vdW) forces despite large lattice mismatches.[1,11] Such vdW heterostructures permit the exploration of artificially structured multilayers composed of 2D crystals with different optical and electronic properties and allow the emergence of new properties. For example, heterojunctions made by the vertical stacking of two monolayer metal dichalcogenides (*e.g.*, WSe_2/MoS_2) resulted in a new photoluminescence (PL) arising from the coupling of the two semiconductor bandgaps.[10] Highly efficient gate-tunable photocurrent was generated from MoS_2/Gr vdW heterostructures.[9] With the use of monolayer *h*BN or MoS_2 as a vertical transport barrier, bipolar field-effect tunneling transistors based on graphene heterostructures have been demonstrated.[2]

So far, such vdW heterostructures have primarily been fabricated by mechanical exfoliation and manual transfer stacking, which could produce crystals with high quality.[7−10] However, this method lacks precise rotational

* Address correspondence to xiaok@ornl.gov.

Received for review March 31, 2015 and accepted July 22, 2015.

Published online July 22, 2015
10.1021/acsnano.5b01943

© 2015 American Chemical Society

control over stacking orientation, usually introduces uncontrollable interface contaminations detrimental to device performance, and is not currently scalable for large-scale device fabrication. Consequently, it is highly preferable to directly grow one type of 2D crystal on another with commensurate stacking through vdW epitaxy. vdW heteroepitaxy of 2D crystals is attracting more and more interest because the self-assembly during growth should result in reproducible, energetically preferred interlayer orientations, more seamless stacking, and clean, sharp interfaces.[12−17]

Gallium selenide (GaSe) is an important layered material in the family of semiconducting metal monochalcogenides (III−VI) and has been widely used in optoelectronics, nonlinear optics, and terahertz radiation detection.[18−20] Recently, our group synthesized large, highly crystalline, triangular GaSe monolayer flakes on SiO_2/Si substrates through a controllable vapor-phase deposition method.[21] The as-synthesized GaSe flakes are highly photoresponsive, with a photoresponsivity of ~1.7 A/W, comparable to exfoliated counterparts,[22] which makes them very favorable potential candidates for photodetectors. By controlling the growth conditions, monolayer GaSe film at wafer scale (~1 cm × 1 cm) can be realized by merging individual triangular flakes together. However, the triangular GaSe flakes grown on amorphous SiO_2 generally show randomly distributed orientations, and therefore, grain boundaries are generally formed when these randomly oriented flakes merge to form larger domains, which will be detrimental to electrical properties of these scaled-up films. Moreover, the low carrier mobility of the 2D GaSe crystals leads to slow response time (generally in milliseconds). Graphene is considered to be a good substrate for the vdW epitaxial growth of other 2D materials[14−17] because of its atomic flatness, surface inertness, lack of dangling bonds, and hexagonal lattice that is typical of *h*BN and metal chalcogenides. These features make graphene a favorable candidate for the vdW epitaxial growth of large area 2D GaSe layers with reduced numbers of grain boundaries. More importantly, graphene exhibits ultrafast photoresponse due to its extremely high carrier mobility and short carrier lifetime.[23] Therefore, GaSe/Gr vdW heterostructures should be expected to combine the advantages of these two materials and potentially give rise to a new material capable of high-speed and highly responsive photodetectors.

In this work, we report the vdW epitaxial growth of 2D GaSe atomic layers on graphene by vapor-phase deposition. Due to the similar hexagonal lattice structure of graphene with GaSe, large single-crystal domains were formed by merging perfectly aligned triangular edges that shared a predominant lattice orientation on graphene. Theoretical analysis reveals that a strong lattice potential corrugation and a small supercell are responsible for the preferred lattice rotation of the GaSe epilayer on graphene. We find that the GaSe crystals grown on graphene show an enhancement of the Raman E^2_{1g} mode due to the enhanced coupling to graphene, and a significant quenching of GaSe photoluminescence stemming from charge transfer from graphene.

RESULTS AND DISCUSSION

The monolayer (1L) graphene used as the template for vdW epitaxy of 2D GaSe crystals was grown through a typical chemical vapor deposition (CVD) process on Cu foil[24] and was subsequently transferred onto a Si substrate with ~250 nm-thermally grown SiO_2 layer using a standard transfer method (see Methods for details). This large area graphene on SiO_2/Si was well suited for the efficient vdW epitaxial growth of GaSe. The optical micrograph (Supporting Information Figure S1a) and SEM image (Supporting Information Figures S1b,c) shows that the transferred graphene clearly had random wrinkles.

The vdW epitaxial growth of GaSe atomic layers on graphene was conducted using a vapor-phase transport and deposition process similar to that described in our previous work.[22] Figure 1a shows a typical optical micrograph of vdW epitaxial GaSe crystals on graphene. Most of the regions with GaSe that are light gray in color are 1L islands as determined by AFM analysis (Figure 1b), while small bilayer (2L) or thicker layered crystals with much brighter contrast also exist (see more AFM images in Supporting Information Figure S2). In stark contrast to the triangular GaSe flakes grown on SiO_2/Si substrates as shown in our previous work,[21] the GaSe flakes grown on graphene are shaped irregularly. The domain sizes of individual monolayer islands are in the range of ~5−60 μm. A longer growth time resulted in larger monolayer GaSe islands, as well as thicker crystals (Supporting Information Figure S3). Figure 1c, d shows scanning electron microscopy (SEM) images of epitaxial GaSe islands (in darker contrast) on graphene during the initial growth stage (*i.e.*, the heating was stopped and gas flow cut off just after the temperature reached 750 °C) and after growth at 750 °C for 5 min, respectively. It is evident that GaSe epilayers start to nucleate and grow from random wrinkles or grain boundaries of the graphene which are indicated by black arrows in Figure 1c, more clearly shown in the inset of Figure 1c, and also by the white arrows indicating the small patches of GaSe bilayers in Figure 1d. Similar preferential nucleation was also observed in the epitaxial growth of MoS_2 and CuPc crystals on graphene at wrinkles and topological defects, where dangling bonds and reactive sites can localize adsorbates.[15,25] As shown in the SEM image of Figure 1e, growth of GaSe monolayers on graphene proceeds by the evolution of sharp edges, each oriented with neighboring contiguous islands at 60° angles. The Raman spectra measured from areas with and without GaSe epilayers

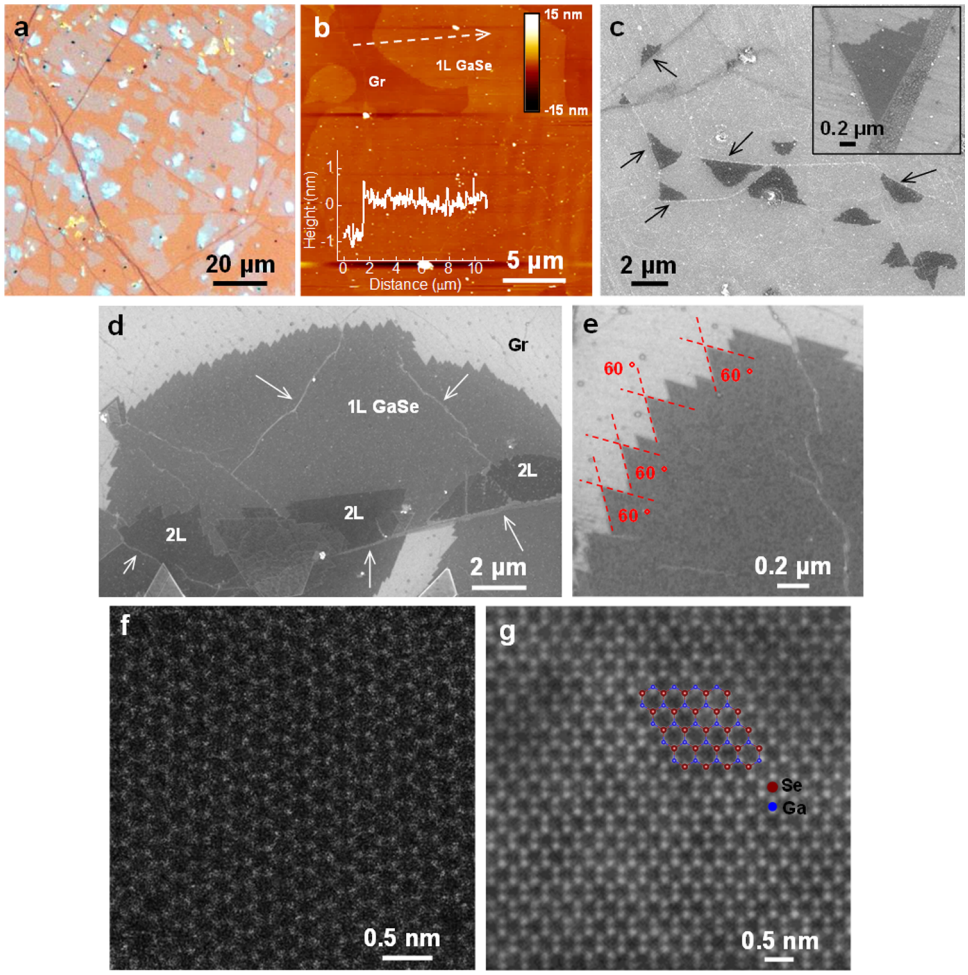

Figure 1. Morphology and structure of 2D GaSe crystals on monolayer graphene. (a) Optical micrograph of GaSe layers on graphene. The regions in gray color are monolayer GaSe, while those with brighter contrast are thicker GaSe crystals. (b) AFM image of 1L GaSe on graphene. Insets are line profiles along the dashed arrow. (c) SEM image of epitaxial monolayer GaSe patches on graphene at the initial growth stage. Inset is an enlarged image showing GaSe starting to grow from random wrinkles or boundaries on graphene. (d) SEM image of an epitaxial GaSe island after 5 min growth, containing mainly 1L with small patches of 2L and thick crystals on graphene. The black and white arrows in (c) and (d) indicate wrinkles or boundaries on graphene. (e) SEM image showing the edge area of 1L GaSe epilayer on graphene. (f and g) Atomic resolution ADF-STEM images of 1L graphene and 1L vdW epitaxial GaSe on graphene, respectively.

are similar (Supporting Information Figure S4), indicating that the GaSe crystal over layer does not appear to affect the quality of the underlying graphene. A broadened D band can be attributed to the carbonization of polymer residue introduced in the transfer process.[26]

To study the crystal structures of the GaSe epilayers and understand the orientation relationship between the GaSe and graphene lattices, the GaSe crystals were directly grown on graphene that was first transferred onto a perforated (2 μm pore size) Si TEM grid covered with 5 nm-thick SiN film (Supporting Information Figure S5), which is similar to the method adopted in recent work.[27] The atomic structures of monolayer graphene (Figure 1f) and monolayer GaSe on graphene (Figure 1g) were imaged using aberration-corrected dark-field scanning transmission electron microscopy (ADF-STEM). Note that it is difficult to resolve the graphene lattice underneath GaSe in Figure 1g because of the intrinsic low contrast arising from a single atomic layer of graphene. Monolayer graphene shows typical hexagonal rings of C atoms with a lattice parameter of ~0.25 nm (Figure 1f), while monolayer GaSe shows hexagonal rings composed of Ga and Se atoms (Figure 1g), in which the distance between two in-plane adjacent Ga (or Se) atoms (as shown by the overlaid top-view schematic in Figure 1g) is ~0.38 nm, matching the lattice parameters of the $a-b$ plane (0.375 nm) in GaSe crystals (note that it is hard to distinguish Ga and Se atoms in the monolayer ADF-STEM image due to their close atomic numbers).

The lattice orientations of GaSe and graphene were investigated using electron diffraction in the transmission electron microscopy (TEM). Figure 2a shows a TEM image of a monolayer GaSe flake on graphene. The selected-area electron diffraction (SAED) pattern along the [001] zone axis acquired from the area contained

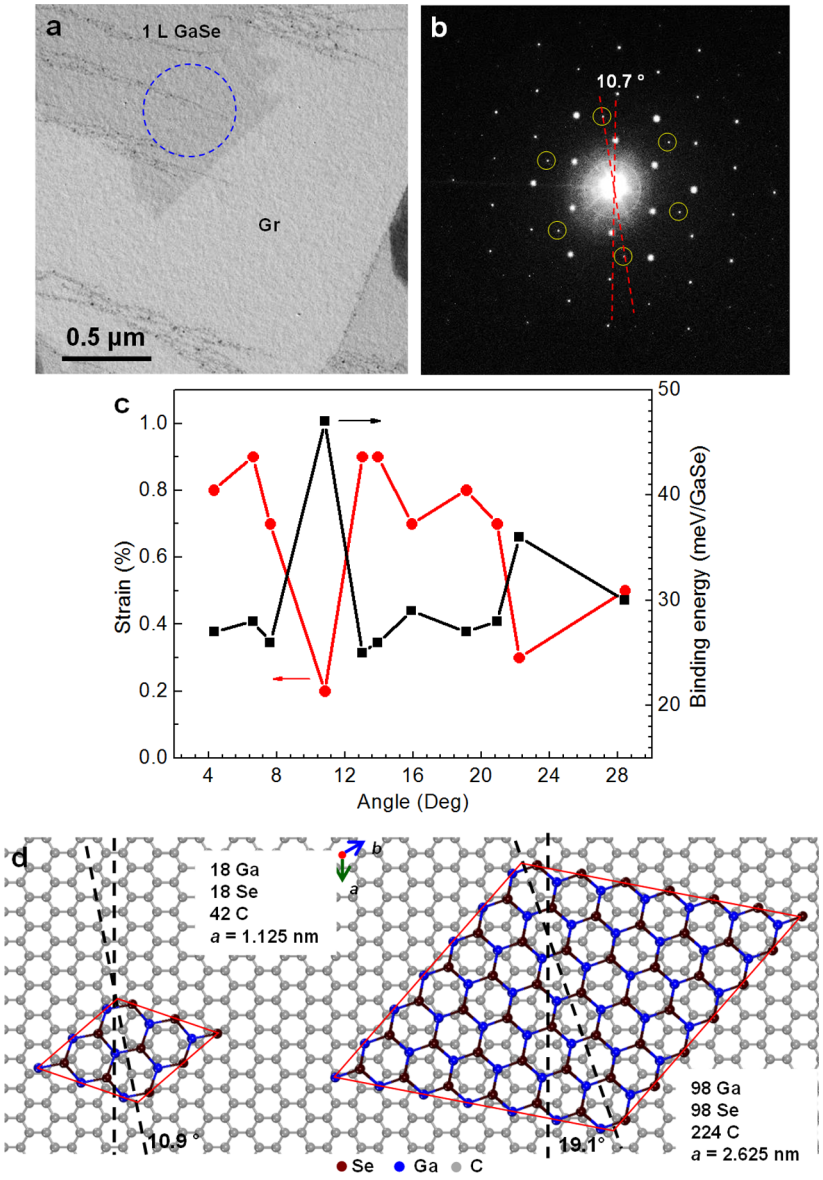

Figure 2. Interlayer lattice rotations between GaSe epilayer and graphene. (a) TEM image of a 1L GaSe grown on CVD-grown 1L graphene. (b) SAED pattern obtained from the region included by dashed circles in (a). The brighter, hexagonally arranged set of diffraction spots is from the GaSe, while the spots with much lower intensity as indicated by yellow circles are from the underlying graphene. The two sets of spots show a rotation angle of ~10°. (c) Residue interlayer strains (red dots) and binding energies (black squares) between 1L graphene and 1L GaSe epitaxial layers as a function of interlayer lattice rotation angles. (d) Schematic illustrations of vdW heterostructure unit cells (supercells) constructed by 1L GaSe epitaxy on 1L graphene with interlayer lattice rotations of 10.9° and 19.1°, respectively.

by the dashed circle in Figure 2a is shown in Figure 2b. The pattern shows two sets of hexagonally arranged (6-fold symmetry) diffraction spots, in which the darker set with longer r (corresponding a = 0.25 nm) comes from the graphene (as highlighted by yellow circles), while the brighter set with shorter r (corresponding to a = 0.38 nm) belongs to the GaSe epilayer. The diffraction patterns shown in this heterostructure indicate that the in-plane lattice parameters of the GaSe epilayer and graphene are similar to their intrinsic bulk value. Interestingly, instead of aligning at the same orientation, the two sets of diffraction spots show a lattice rotation of 10.7° as shown in Figure 2b. After examining the single-crystal GaSe domains in other regions, we found that almost all of the diffraction patterns exhibit interlayer lattice rotations between the epitaxial layer of GaSe and underlying graphene. A rotation angle of 10.5 ± 0.3° was the most commonly observed (~50% of all the crystals examined). The remaining crystalline patches were oriented at various discrete angles ranging between 2 and 28° relative to the underlying graphene (Supporting Information Figure S6). The results are in contrast to other previously reported vdW epitaxial 2D crystals, *e.g.*, *h*BN and WSe_2, on graphene[12,17] where two lattices are generally aligned in the same orientation (note that interlayer

lattice rotations within ~18° were also observed between MoS_2 and graphene[14]). The similarity of the in-plane lattice parameters to their intrinsic bulk values together with the preferred alignment between the GaSe epilayer and graphene layer suggests that the growth indeed occurs *via* vdW epitaxy despite the large lattice mismatch (~58%).[28]

To understand the preferred interlayer lattice rotation of GaSe epilayer relative to graphene, we performed density functional theory (DFT) calculations of GaSe-covered graphene. The vdW epitaxy of GaSe on graphene with certain interlayer rotations leads to new long-range ordered superstructures with repeating units (supercells). To discover viable supercells during the simulation, different lattice mismatches were introduced for different rotation angles. For a few specific rotation angles, we discovered several viable supercells containing less than 2000 atoms corresponding to GaSe lattice strains of less than 1% that are still predicted to remain bound to graphene (Figure 2c, see Supporting Information for details). Remarkably, these calculated angles are in good agreement with those observed experimentally (Figure 2b and Supporting Information Figure S6). More importantly, among these calculated rotation angles, the 10.9° rotation angle results in the smallest supercell size (containing 18 Ga and 18 Se and 48 C atoms) with a lattice constant a = 1.125 nm, which also corresponds to the structure with the smallest strain ~0.2%. Note that the supercells are not obvious to the eye because of the large mismatch between GaSe and graphene lattice constants (3 and 4.6 times, respectively) (Figure 2d, left cell). Other rotation angles found correspond to larger supercells (Figure 2d and others shown in Supporting Information Figure S7) with larger strains and smaller binding energies (Figure 2c). For different rotation angles, the binding energies are inhomogeneous and in the range of ~25−36 meV/GaSe except for the 10.9° rotation angle which displays a significantly larger binding energy of 47 meV/GaSe. The calculated binding energies (shown in Figure 2c, black squares) are expressed in terms of the total energies per GaSe pair compared to the total energies of separated GaSe and graphene, and include the strain energy. Therefore, the supercell with 10.9° interlayer rotation is predicted to be the energetically most stable structure.

This predicted energetically preferred orientation of 10.9° is in good agreement with that observed experimentally (*i.e.*, 10.5 ± 0.3°). The fact that a high fraction (~50%) of crystals appear to follow the energetically preferred orientation dictated by the graphene lattice implies both vdW epitaxy and that orientation is determined early in the growth of the crystalline flake, since the binding energy of a flake increases with the number of GaSe pairs. The ability of a flake to diffuse or rotate can be estimated by the difference in its binding energy between different orientations as compared to k_BT (considering the degree of freedom of a 2D flake bound on the substrate), where k_B is the Boltzmann constant and T is the system temperature. As the flakes grow in size, the difference between the binding energy of the 10.9° rotation and that of the other rotation angles increases linearly with the number of atoms in the flake. For example, at the growth temperature of 700 °C (corresponding to k_BT = 83 meV), the calculations predict that all rotation angles are experimentally accessible for the assembly of the first few GaSe pairs. However, as the flakes grow in size, the probability of forming the 10.9° rotation increases exponentially based on Arrhenius behavior. After the binding energy of the flakes exceeds energies of a few k_BT, the crystals should be effectively pinned in a particular orientation. Therefore, the crystal orientation should be determined by the competition between the growth rate and the diffusion rate of the flake on the substrate as it samples the surface potential corrugation for the most stable orientation.

The preferred lattice orientation of GaSe epilayers on graphene is very different from our previous growth of GaSe on amorphous SiO_2/Si substrates, in which all the crystalline, triangular GaSe flakes show a random orientation and clear grain boundaries result when they merge to form larger domains.[21,29] In addition to the lack of an identifiable supercell on amorphous SiO_2, one could expect that the diffusion coefficient could be quite different compared to that on graphene, as large quantities of surface defects on amorphous SiO_2 surfaces may trap and immobilize adsorbed GaSe molecules.

As described above, the edges of the monolayer GaSe on graphene consist of 60° triangles aligned at the same orientation (Figure 1e). When examined by TEM, as shown in Figure 3a, similar 60° triangular edges can be seen on much shorter length scales. SAED patterns obtained from neighboring crystals in the edge (as indicated by dashed circles 1 and 2 in Figure 3a) are given in Figures 3b,c, and are compared with Figure 3d, which shows the SAED pattern from the inner area of the domain (as indicated by dashed circle 3 in Figure 3a). All three patterns show exactly the same set of diffraction spots with 6-fold symmetry, and a ~10.7° (preferred orientation) lattice rotation with respect to graphene. Therefore, the GaSe islands at the edge have the same lattice orientation with the inner regions of the single crystal domains. The same results were also obtained from edge and inner areas of 1L single crystal GaSe domains with other lattice orientations, *e.g.*, 15° and 20° relative to graphene (Supporting Information Figures S8 and S9). These results indicate that large (tens of microns) irregularly shaped, single-crystalline GaSe epilayer domains grow, after preferential nucleation on random wrinkles or grain boundaries of graphene, by the merging of well-aligned, yet

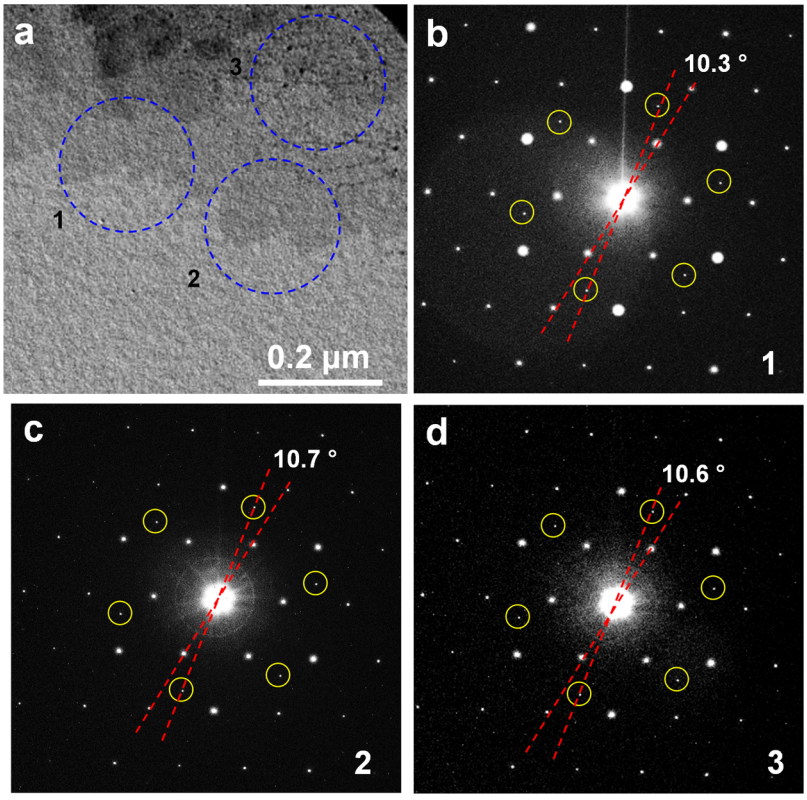

Figure 3. Epitaxy of single-crystalline GaSe on graphene. (a) TEM image showing the area near the edge of vdW epitaxial GaSe islands on graphene. (b–d) SAED patterns obtained from regions 1, 2, and 3 included in the dashed circles in (a).

irregular, triangular edges oriented at 60° that share a preferred lattice orientation with underlying graphene. Such growth of large 2D crystals with same lattice orientation were also recently reported on vdW epitaxial MoS_2 on *c*-plane sapphire substrate.[30]

In addition to 1L GaSe on graphene, few-layer GaSe flakes, as shown in Figure 1a and Supporting Information Figure S2, were also investigated. Interestingly, few-layer 2D crystals have attracted much interest recently because of their richer electronic and optical properties when compared to monolayer systems due to the fact that different interlayer orientations and stacking modes lead to different electronic structures.[10,31−33] Figure 4a,b shows the TEM images of two trilayer GaSe islands on graphene, in which two different interlayer orientations are identified. In Figure 4a, the second and first layer show 60° interlayer rotation (60°-2L), while the third and second layer are at the same orientation (60−0°-3L); in Figure 4b, all the three layers are stacked at the same orientation (0°-2L and 0−0°-3L). Z-contrast ADF-STEM imaging directly images the atomic structures of the 60°-2L (Supporting Information Figures 4c and S10a), 0°-2L (Figure 4f and Supporting Information Figure S10b), 60−0°-3L (Figure 4i and Supporting Information Figure S10c), and 0−0°-3L (Figure 4l and Supporting Information Figure S10d) stackings shown in Figure 4a,b. Corresponding quantitative simulations of the Z-contrast ADF images are shown in Figures 4d,g,j,m, respectively. Intensity profiles for experimental (scatters dots) and simulation (solid curves) images are consistent with each other, as displayed in Figure 4e,h,k,n. The results indicate that the 60°-2L has a 2H-type stacking, belonging to the β-prototype GaSe, the 0°-2L has a 2R-type stacking, belonging to the ε-prototype GaSe, the 60−0°-3L has a 2H-2R-type stacking, corresponding to δ-prototype GaSe, and the 0−0°-3L has a 3R-type stacking, belonging to γ-prototype GaSe. The results show that all of the four prototype structures of GaSe can be obtained in the GaSe epilayers on graphene. The fact that few-layer GaSe grown on graphene maintained structures corresponding to bulk GaSe crystals further confirms the vdW epitaxial growth of GaSe atomic layers on graphene since the layer-by-layer growth of GaSe was not influenced by the large lattice mismatch between graphene and epitaxial layers. Moreover, directly relating the interlayer orientations with stacking modes provides a useful guide to study the electronic structures of these differently stacked few-layer GaSe crystals.

The optical properties of the vdW epitaxial GaSe layers on graphene were studied using Raman and PL spectroscopy. The Raman and PL spectra were acquired using 532 nm laser excitation through a microscope equipped with a long distance objective (~1 μm spot size) in backscattering configuration. Figure 5a shows the Raman spectra (80−400 cm^{-1}) acquired from the vdW epitaxial GaSe crystals with ~10L,

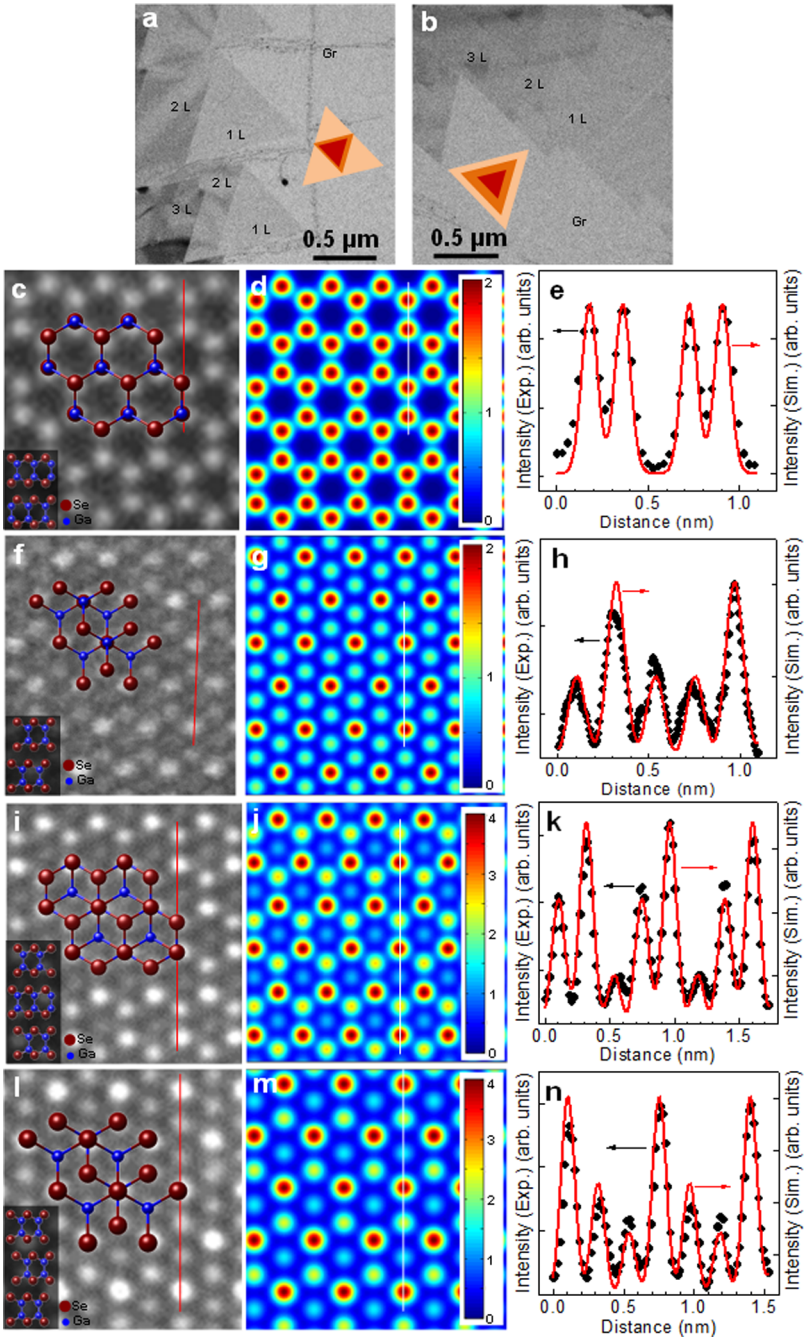

Figure 4. Atomic resolution structures of bilayer and trilayer GaSe crystals with different stacking modes on graphene. (a and b) TEM images of GaSe crystals showing 1L, 2L, and 3L regions with different interlayer rotations. (c) ADF-STEM images obtained from 2L GaSe region in (a), showing a 2H stacking. (d) Simulated ADF image of 2L GaSe with the 2H stacking. (e) Intensity profiles along the solid line in the ADF-STEM image in (c) (scattered dots) and the solid line in the simulated ADF image in (d) (solid curve). (f) ADF-STEM images obtained from 2L GaSe region in (b), showing a 2R stacking. (g) Simulated ADF image of 2L GaSe with the 2R stacking. (h) Intensity profiles along the solid line in the ADF-STEM image in (g) (scattered dots) and the solid line in the simulated ADF image in (h) (solid curve). (i) ADF-STEM images obtained from 3L GaSe region in (a), showing a 2H−2R stacking. (j) Simulated ADF image of 3L GaSe with the 2H−2R stacking. (k) Intensity profiles along the solid line in the ADF-STEM image in (i) (scattered dots) and the solid line in the simulated ADF image in (j) (solid curve). (l) ADF-STEM images obtained from 3L GaSe region in (b), showing a 3R stacking. (m) Simulated ADF image of 3L GaSe with the 3R stacking. (n) Intensity profiles along the solid line in the ADF-STEM image in (l) (scattered dots) and the solid line in the simulated ADF image in (m) (solid curve). In panels c, f, i, and l, top view and side views of the 2H, 2R, 2H−2R, and 3R stacking are overlaid, respectively.

~ 7L, 3L, and 1L grown on SiO_2/Si substrates. The Raman spectrum from the graphene area on a SiO_2/Si substrate without GaSe is also presented, showing the characteristic 304 cm^{-1} Si Raman peak from the substrate (Figure 5a, black curve). The Raman spectrum of the crystal with ~10 L shows characteristic peaks of GaSe corresponding to A^1_{1g} (~135 cm^{-1}), E^1_{2g} (~208 cm^{-1}), and A^2_{1g} (~311 cm^{-1}) vibrational modes

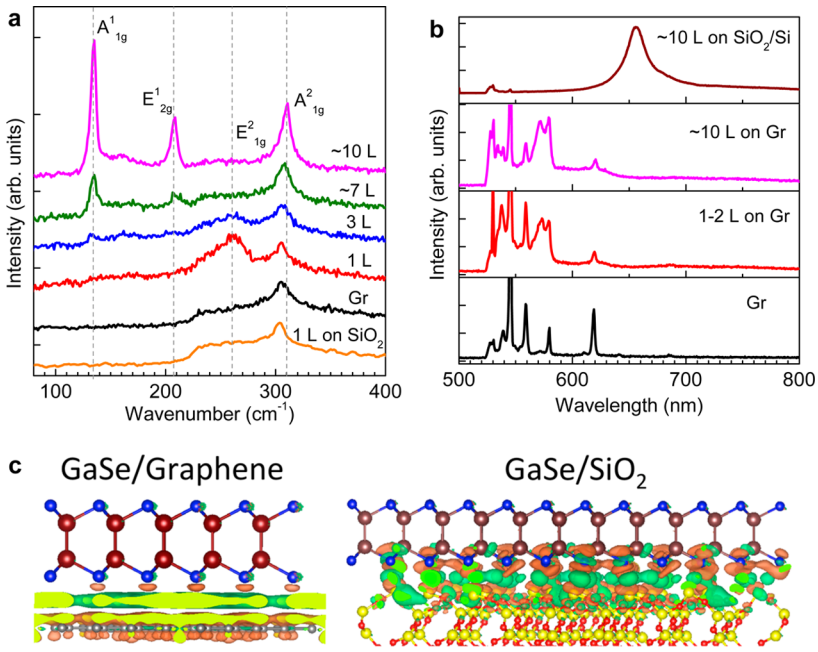

Figure 5. Optical properties of 2D GaSe epilayers on graphene. (a) Raman spectra (with 532 nm laser excitation) of GaSe crystals with ~10L (magenta curve), ~7L (green curve), 3L (blue curve), and 1L (red curve). The black curve is acquired from the graphene area without GaSe grown on it. The orange curve stands for the 1L GaSe crystal grown on SiO_2/Si. Note that the spectra were offset for clarity. (b) PL spectra of 2D GaSe crystals grown on graphene and SiO_2/Si substrates. Brown curve, a ~10L crystal on SiO_2/Si; magenta curve, a ~10L crystal grown on Gr; red curve, a 1L crystal on Gr; black curve, graphene area without any crystal grown on it. (c) Changes in charge density upon adsorption of GaSe on the substrates, with isosurface of 0.001e/Å^3 for GaSe on Graphene and 0.005e/Å^3 for GaSe on SiO_2, where green color is for electron accumulation and orange color for electron depletion.

(Figure 5a, magenta curve).[20,34,35] The intensity of the three peaks decreases prominently as the GaSe layers are thinned. The A^1_{1g} and E^1_{2g} peaks can hardly be detected for 1L crystals (Figure 5a, red curve). The A^1_{1g} and A^2_{1g} peaks (out-of-plane modes) show red-shifts as the layer number decreases, *i.e.*, the A^1_{1g} peak shifts to ~131 cm^{-1} for 3L crystals (Figure 5a, blue curve) and the A^2_{1g} peak shifts to ~308 cm^{-1} for ~7L crystals (Figure 5a, green curve), which is due to the weakening of the interlayer interactions in GaSe when the number of layers decreases. However, a very prominent difference for GaSe epilayer on graphene and GaSe on SiO_2 substrate is the enhancement of E^2_{1g} Raman peak as the layer number decreases. The E^2_{1g} vibration mode, generally peaking at ~244 cm^{-1} for very thick (>30L) GaSe crystals,[20] is not detected in GaSe crystals with ~7−10L (Figure 5a, green and magenta curves). It, however, shows up at ~261 cm^{-1} when the crystal contains less than 7L (Figure 5a, blue and red curves), and is most intense in the case of 1L GaSe. Such a phenomenon was not observed in the 2D GaSe crystals grown directly on SiO_2/Si substrates (Figure 5a, orange curve).[20,34,35] The enhanced in-plan E^2_{1g} mode for the first several GaSe epilayers could result from the strong charge transfer between graphene and GaSe epilayers. This phenomenon has also been demonstrated by previous studies that the enhancement of the Raman spectra of adsorbed organic molecules on graphene comes from the charge transfer between graphene and the organic molecules.[36,37] The influence of the underlying graphene on the optical properties of vdW epitaxial GaSe layers is also evident from their PL spectra. Note that in the case of GaSe PL intensity drops rapidly as the thickness decreases below ~10L and is undetectable in a few layer GaSe, which is probably due to the direct-to-indirect bandgap transition with decreasing layer number of 2D GaSe, as calculated in our previous work.[21] As shown in Figure 5b, the PL from the GaSe epilayers on graphene in the case of 10L GaSe crystals is significantly quenched compared with that on SiO_2/Si substrates. A possible mechanism for this quenching effect is fast decay of excitons followed by electron transfer to graphene. Such a graphene-induced quenching of PL has also been observed in the case of monolayer MoS_2 grown on graphene[16] and graphene-semiconductor quantum dots systems.[38]

To understand the magnitude of the charge transfer between graphene and GaSe, theoretical calculations were conducted to determine charge density using DFT and a Bader analysis algorithm.[39] The results show that the charge transfer from GaSe to graphene (in the case of a 10.9° interlayer rotation) is 0.484e (~2.84 × 10^{13} cm^{-2}), which is significantly larger than that from GaSe to a crystalline SiO_2 substrate (0.068e (~4 × 10^{12} cm^{-2})). Moreover, Figure 5c reveals the qualitatively different nature of the spatial charge reorganization in these two cases. For GaSe/SiO_2, significant charge

rearrangement is induced at the interface but it is highly localized, and when averaged, the electron- and hole-accumulation regions result in the small net directional charge transfer. On the contrary, for GaSe/graphene no significant charge rearrangement is induced locally at the GaSe/graphene interface; however, electrons are exclusively accumulated at the interface while the holes remain distributed nearly entirely on the graphene layer, resulting in a much larger directional charge transfer.

CONCLUSIONS

In summary, despite significant mismatch between GaSe and graphene lattices, from our experiments and theoretical calculations we conclude that energetically preferred orientations exist to drive the growth of high-quality, large single-crystalline 2D GaSe domains by vdW epitaxy. Electron diffraction of GaSe epilayers on graphene directly characterized the interlayer stacking configurations, finding the lattice rotation angle of $10.5 \pm 0.3°$ as the most frequent vdW heterostructure, in agreement with the theoretical finding (10.9°) of this orientation as the one with the smallest supercell of the lowest strain and the strongest binding energy. Although random wrinkles or boundaries in the graphene were found to be the preferred nucleation sites and growth of the large GaSe domains was observed to proceed from the free edges, the strong tendency to energetically conform to the underlying graphene lattice indicates that the domain orientation is likely determined during the nucleation stage, before the flake becomes pinned to the substrate. Theoretical calculations of the interlayer energetics support the experimental observations that the large single crystal GaSe epilayers are formed through the coalescence of perfectly aligned triangular edges in this most energetically favored stacking. Although ~50% of structures adopted this energetically favorable configuration, methods will need to be developed to suppress other metastable orientations (especially during nucleation) to guarantee the synthesis of mesoscale single crystal vdW heterostructures. Strong photoluminescence quenching in the GaSe/Gr vdW heterostructures indicates strong charge transfer between the GaSe and graphene which may be beneficial for photodetectors. Thus, vdW epitaxy of GaSe on graphene provides a synthetic technique for the fabrication of large-area, single-crystal domains for heterostructures with excellent interfacial properties for optoelectronics.

METHODS

Synthesis of GaSe Bulk Crystals. Ga_2Se_3 (99.99%, Alfa Aesar) and Ga (99.99%, Alfa Aesar) were mixed at a molar ratio of 1:1 and then sealed in an evacuated quartz tube under $<10^{-3}$ Torr of argon. The mixture was heated to 950 °C (from 25 to 700 °C in 35 min and from 700 to 950 °C in 25 min) and maintained at temperature for 1 h. After heating, the system was cooled down first to 850 °C in 2 h and then naturally to room temperature.

Synthesis and Transfer of Monolayer Graphene. Graphene was grown as described earlier.[24] In brief, electropolished 125 μm thick copper foils were loaded into atmospheric pressure CVD reactor and annealed at 1065 °C under the flow of 2.5% H_2 in Ar for 30 min. Graphene growth was performed by addition of methane with a gradual increase of concentration from 10 to 20 to 40 ppm for 30 min increments. After growth, a Micro Chem PMMA 495A4 solution was spin-coated at 2000 rpm onto the sample. Graphene from the back side of the copper was etched away by oxygen plasma and copper was dissolved by 1 M $FeCl_3$ in 3% HCl, leaving a graphene/PMMA floating sandwich. This was then washed with DI water and transferred to the substrate of interest. PMMA was dissolved in acetone with subsequent annealing at 550 °C to remove PMMA residues.

vdW Epitaxial Growth of 2D GaSe Crystals. The vdW epitaxy of 2D GaSe crystals on the as grown and transferred graphene was carried out in a tube furnace system equipped with a 1 in. quartz tube. Bulk GaSe crystals and Ga_2Se_3 powder were mixed together (GaSe/Ga_2Se_3 molar ratio ~50:1), and were used as source materials. In a typical run, ~60 mg of source powder and a piece of SiO_2 (~250 nm)/Si substrate (2 cm long and 1 cm wide) covered with graphene were loaded on a quartz boat, and subsequently inserted into the furnace. The source was located at the center of the furnace, with the substrate located ~8−10 cm downstream. After evacuating the tube to ~5×10^{-3} Torr, the reaction was conducted at 750 °C (with a ramping rate of 20 °C/min) for 5 min at a pressure of 30 Torr and an argon carrier gas flow rate of 30 sccm. The vapor-phase reactants were transported by the flowing argon gas to the growth region, in which the temperature was ~710−720 °C, thereby feeding the growth of the 2D GaSe crystals. After growth, the furnace was cooled naturally to room temperature.

Characterization. The morphologies of the vdW epitaxial 2D GaSe on graphene were characterized using optical microscopy (Leica DM4500 P), SEM (Zeiss Merlin SEM), and AFM (Bruker Dimension Icon AFM).

The atomic-resolution structures of the vdW epitaxial 2D GaSe crystals were investigated using ADF-STEM, and the interlayer lattice rotation between GaSe and graphene were investigated using SAED in TEM. The ADF-STEM image was obtained using an aberration-corrected Nion UltraSTEM operating at 60 kV, using a half an gle range of the ADF detector from 86 to 200 mrad. TEM imaging and SAED were conducted using an FEI Technai T12 at 100 kV at low dose densities, and no detectable damage was observed during imaging. The samples for STEM and TEM analysis were directly grown on the monolayer graphene that was first transferred onto Si TEM grids covered by 5 nm-thick amorphous SiN film with 2 μm windows.

Raman and PL measurements were performed using a continuous wave laser (1 mW laser power, λ = 532 nm) through a microscope of a micro-Raman system (Jobin Yvon Horiba, T6400) focused to a spot of ~1 μm using a long distance objective (100× N/A = 0.8). The Raman (or PL) signal was collected through the same objective in backscattering configuration and focused onto a slit of a single stage of the triple-monochromator equipped with a liquid nitrogen cooled CCD camera and 900 grooves/mm grating.

Theoretical Calculation. All the density functional theory (DFT) calculations were performed using the VASP code.[40] Projector augmented wave potentials was used to describe the core electrons, and the generalized gradient approximation (GGA) with the Perdew−Burke−Ernzerhof (PBE) functional was selected in our calculations. The effect of vdW interactions was taken into account by using the PBE + vdW.[41] The kinetic energy cut for the plane-wave basis was set to 400 eV. The structure was fully relaxed until the force on each atom was less than 0.02 eV/A.

Conflict of Interest: The authors declare no competing financial interest.

Acknowledgment. Synthesis science and theoretical studies sponsored by the Materials Science and Engineering Division, Office of Basic Energy Sciences, U.S. Department of Energy. Materials characterization conducted at the Center for Nanophase Materials Sciences, which is sponsored at Oak Ridge National Laboratory by the Scientific User Facilities Division, Office of Basic Energy Sciences, U.S. Department of Energy. L.B. acknowledges the financial support of the National Secretariat of Higher Education, Science, Technology and Innovation of Ecuador (SENESCYT). J.L. acknowledges support from ORNL Laboratory Directed Research and Development. This research used resources of the National Energy Research Scientific Computing Center, which is supported by the Office of Science of the US DOE (contract no. DE-AC02-05CH11231).

Supporting Information Available: Optical micrographs, SEM, AFM, and TEM images of graphene and GaSe epilayers grown on graphene, SAED patterns of GaSe/graphene, schematic illustrations of GaSe/graphene supercells, Raman spectra of graphene, and ADF-STEM images of 2L and 3L GaSe on graphene. The Supporting Information is available free of charge on the ACS Publications website at DOI: 10.1021/acsnano.5b01943.

REFERENCES AND NOTES

1. Geim, A. K.; Grigorieva, I. V. Van der Waals Heterostructures. *Nature* **2013**, *499*, 419–425.
2. Britnell, L.; Gorbachev, R. V.; Jalil, R.; Belle, B. D.; Schedin, F.; Mishchenko, A.; Georgiou, T.; Katsnelson, M. I.; Eaves, L.; Morozov, S. V.; et al. A. Field-Effect Tunneling Transistor Based on Vertical Graphene Heterostructures. *Science* **2012**, *335*, 947–950.
3. Dean, C. R.; Young, A. F.; Meric, I.; Lee, C.; Sorgenfrei, S.; Watanabe, K.; Taniguchi, T.; Kim, P.; Shepard, K. L.; Hone, J. Boron Nitride Substrates for High-Quality Graphene Electronics. *Nat. Nanotechnol.* **2010**, *5*, 722–726.
4. Ponomarenko, L. A.; Geim, A. K.; Zhukov, A. A.; Jalil, R.; Morozov, S. V.; Novoselov, K. S.; Grigorieva, I. V.; Hill, E. H.; Cheianov, V. V.; Fal'ko, V. I.; et al. Tunable Metal-Insulator Transition in Double-Layer Graphene Heterostructures. *Nat. Phys.* **2011**, *7*, 958–961.
5. Gorbachev, R. V.; Geim, A. K.; Katsnelson, M. I.; Novoselov, K. S.; Tudorovskiy, T.; Grigorieva, I. V.; MacDonald, A. H.; Morozov, S. V.; Watanabe, K.; Taniguchi, T.; et al. Strong Coulomb Drag and Broken Symmetry in Double-Layer Graphene. *Nat. Phys.* **2012**, *8*, 896–901.
6. Zhang, K.; Yap, F. L.; Li, K.; Ng, C. T.; Li, L.; Loh, K. P. Large Scale Graphene/Hexagonal Boron Nitride Heterostructure for Tunable Plasmonics. *Adv. Funct. Mater.* **2014**, *24*, 731–738.
7. Georgiou, T.; Jalil, R.; Belle, B. D.; Britnell, L.; Gorbachev, R. V.; Morozov, S. V.; Kim, Y. − J.; Gholinia, A.; Haigh, S. J.; Makarovsky, O.; et al. Vertical Field-Effect Transistor Based on Graphene-WS_2 Heterostructures for Flexible and Transparent Electronics. *Nat. Nanotechnol.* **2013**, *8*, 100–103.
8. Roy, K.; Padmanabhan, M.; Goswami, S.; Sai, T. P.; Ramalingam, G.; Raghavan, S.; Ghosh, A. Graphene-MoS_2 Hybrid Structures for Multifunctional Photoresponsive Memory Devices. *Nat. Nanotechnol.* **2013**, *8*, 826–830.
9. Yu, W. J.; Liu, Y.; Zhou, H. L.; Yin, A. X.; Li, Z.; Huang, Y.; Duan, X. F. Highly Efficient Gate-Tunable Photocurrent Generation in Vertical Heterostructures of Layered Materials. *Nat. Nanotechnol.* **2013**, *8*, 952–958.
10. Fang, H.; Battaglia, C.; Carraro, C.; Nemsak, S.; Ozdol, B.; Kang, J. S.; Bechtel, H. A.; Desai, S. B.; Kronast, F.; Unal, A. A.; et al. A. Strong Interlayer Coupling in van der Waals Heterostructures Built from Single-Layer Chalcogenides. *Proc. Natl. Acad. Sci. U. S. A.* **2014**, *111*, 6198–6202.
11. Gao, G. H.; Gao, W.; Cannuccia, E.; Taha-Tijerina, J.; Balicas, L.; Mathkar, A.; Narayanan, T. N.; Liu, Z.; Gupta, B. K.; Peng, J.; et al. Artificially Stacked Atomic Layers: Toward New van der Waals Solids. *Nano Lett.* **2012**, *12*, 3518–3525.
12. Yang, W.; Chen, G. R.; Shi, Z. W.; Liu, C. − C.; Zhang, L. C.; Xie, G. B.; Cheng, M.; Wang, D. M.; Yang, R.; Shi, D. X.; et al. Epitaxy Growth of Single-Domain Graphene on Hexagonal Boron Nitride. *Nat. Mater.* **2013**, *12*, 792–797.
13. Roth, S.; Matsui, F.; Greber, T.; Osterwalder, J. Chemical Vapor Deposition and Characterization of Aligned and Incommensurate Graphene/Hexagonal Boron Nitride Heterostack on Cu(111). *Nano Lett.* **2013**, *13*, 2668–2675.
14. Shi, Y. M.; Zhou, W.; Lu, A. − Y.; Fang, W. J.; Lee, Y. − H.; Hsu, A. L.; Kim, S. M.; Kim, K. K.; Yang, H. Y.; Li, L. − J.; et al. van der Waals Epitaxy of MoS_2 Layers Using Graphene as Growth Templates. *Nano Lett.* **2012**, *12*, 2784–2791.
15. Lin, Y. − C.; Lu, N.; Perea-Lopez, N.; Li, J.; Lin, Z.; Peng, X.; Lee, C. H.; Sun, C.; Calderin, L.; Browning, P. N.; et al. Direct Synthesis of van der Waals Solids. *ACS Nano* **2014**, *8*, 3715–3723.
16. Ago, H.; Endo, H.; Solís-Fernández, P.; Takizawa, R.; Ohta, Y.; Fujita, Y.; Yamamoto, K.; Tsuji, M. Controlled van der Waals Epitaxy of Monolayer MoS_2 Triangular Domains on Graphene. *ACS Appl. Mater. Interfaces* **2015**, *7*, 5265–5273.
17. Lin, Y. − C.; Chang, C. − Y. S.; Ghosh, R. K.; Li, J.; Zhu, H.; Addou, R.; Diaconescu, B.; Ohta, T.; Peng, X.; Lu, N.; et al. Atomically Thin Heterostructures Based on Single-Layer Tungsten Diselenide and Graphene. *Nano Lett.* **2014**, *14*, 6936–6941.
18. Leontie, L.; Evtodiev, I.; Nedeff, V.; Stamate, M.; Caraman, M. Photoelectric Properties of Bi_2O_3/GaSe Heterojunctions. *Appl. Phys. Lett.* **2009**, *94*, 071903.
19. Shi, W.; Ding, Y. J.; Fernelius, N.; Vodopyanov, K. Efficient, Tunable, and Coherent 0.18−5.27-THz Source Based on GaSe Crystal. *Opt. Lett.* **2002**, *27*, 1454.
20. Allakhverdiev, K. R.; Yetis, M. Ö.; Özbek, S.; Baykara, T. K.; Salaev, E. Y. Effective Nonlinear GaSe Crystal. Optical Properties and Applications. *Laser Phys.* **2009**, *19*, 1092–1104.
21. Li, X. F.; Lin, M. − W.; Puretzky, A. A.; Idrobo, J. C.; Ma, C.; Chi, M. F.; Yoon, M.; Rouleau, C. M.; Kravchenko, I. I.; Geohegan, D. B.; et al. Controlled Vapor Phase Growth of Single Crystalline, Two-Dimensional GaSe Crystals with High Photoresponse. *Sci. Rep.* **2014**, *4*, 5497.
22. Hu, P. A.; Wen, Z. Z.; Wang, L. F.; Tan, P. H.; Xiao, K. Synthesis of Few-Layer GaSe Nanosheets for High Performance Photodetectors. *ACS Nano* **2012**, *6*, 5988–5994.
23. Xia, F. N.; Mueller, T.; Lin, Y. − M.; Valdes-Garcia, A.; Avouris, P. Ultrafast Graphene Photodetector. *Nat. Nanotechnol.* **2009**, *4*, 839–843.
24. Vlassiouk, I.; Smirnov, S.; Regmi, M.; Surwade, S. P.; Srivastave, N.; Feenstra, R.; Eres, G.; Parish, C.; Lavrik, N.; Datskos, P.; et al. Graphene Nucleation Density on Copper: Fundamental Role of Background Pressure. *J. Phys. Chem. C* **2013**, *117*, 18919–18926.
25. Xiao, K.; Deng, W.; Keum, J. K.; Yoon, M.; Vlassiouk, I. V.; Clark, K. W.; Li, A. − P.; Kravchenko, I. I.; Gu, G.; Payzant, E. A.; et al. Surface-Induced Orientation Control of CuPc Molecules for the Epitaxial Growth of Highly Ordered Organic Crytals on Graphene. *J. Am. Chem. Soc.* **2013**, *135*, 3680–3687.
26. Hong, J.; Park, M. K.; Lee, E. J.; Lee, D.; Hwang, D. S.; Ryu, S. Origin of New Broad Raman D and G peaks in Annealed Graphene. *Sci. Rep.* **2013**, *3*, 2700.
27. Azizi, A.; Eichfeld, S.; Geschwind, G.; Zhang, K. H.; Jiang, B.; Mukherjee, D.; Hossain, L.; Piasecki, A. F.; Kabius, B.; Robinson, J. A.; et al. Freestanding van der Waals Heterostructures of Graphene and Transition Metal Dichalcogenides. *ACS Nano* **2015**, *9*, 4882.
28. Koma, A. Van der Waals Epitaxy for Highly Lattice-Mismatched Systems. *J. Cryst. Growth* **1999**, *201−202*, 236–241.
29. Mahjouri-Samani, M.; Tian, M.; Wang, K.; Boulesbaa, A.; Rouleau, C. M.; Puretzky, A. A.; McGuire, M. A.; Srijanto, B. R.; Xiao, K.; Eres, G.; et al. Digital Transfer Growth of Patterned 2D Metal Chalcogenides by Confined Nanoparticle Evaporation. *ACS Nano* **2014**, *8*, 11567–11575.
30. Dumcenco, D.; Ovchinnikov, D.; Marinov, K.; Lazić, P.; Gibertini, M.; Marzari, N.; Sanchez, O. L.; Kung, Y. − C.; Krasnozhon, D.; Chen, M. − W.; et al. Large-Area Epitaxial Monolayer MoS_2. *ACS Nano* **2015**, *9*, 4611–4620.
31. Liu, K. H.; Zhang, L. M.; Cao, T.; Jin, C. H.; Qiu, D.; Zhou, Q.; Zettl, A.; Yang, P. D.; Louie, S. G.; Wang, F. Evolution of

Interlayer Coupling in Twisted Molybdenum Disulfide Bilayers. *Nat. Commun.* **2014**, *5*, 4966.
32. Wu, S. F.; Ross, J. S.; Liu, G. − B.; Aivazian, G.; Jone, A.; Fei, Z. Y.; Zhu, W. G.; Xiao, D.; Yao, W.; Cobden, D.; et al. Electrical Tuning of Valley Magnetic Moment Through Symmetry Control in Bilayer MoS_2. *Nat. Phys.* **2013**, *9*, 149–153.
33. Li, X. F.; Basile, L.; Yoon, M.; Ma, C.; Puretzky, A. A.; Lee, J.; Idrobo, J. C.; Chi, M. F.; Rouleau, C. M.; Geohegan, D. B.; et al. Revealing the Preferred Interlayer Orientations and Stackings of Two-Dimensional Bilayer Gallium Selenide Crystals. *Angew. Chem., Int. Ed.* **2015**, *54*, 2712–2717.
34. Lei, S. D.; Ge, L. H.; Liu, Z.; Najmaei, S.; Shi, G.; You, G.; Lou, J.; Vajtai, R.; Ajayan, P. M. Synthesis and Photoresponse of Large GaSe Atomic Layers. *Nano Lett.* **2013**, *13*, 2777–2781.
35. Zhou, Y. B.; Nie, Y. F.; Liu, Y. J.; Yan, K.; Hong, J. H.; Jin, C. H.; Zhou, Y.; Yin, J. B.; Liu, Z. F.; Peng, H. L. Epitaxy and Photoresponse of Two-Dimensional GaSe Crystals on Flexible Transparent Mica Sheets. *ACS Nano* **2014**, *8*, 1485–1490.
36. Ling, X.; Xie, L. M.; Fang, Y.; Xu, H.; Zhang, H. L.; Kong, J.; Dresselhaus, M. S.; Zhang, J.; Liu, Z. F. Can Graphene be Used as a Substrate for Raman Enhancement?. *Nano Lett.* **2010**, *10*, 553–561.
37. Ling, X.; Fang, W. J.; Lee, Y. − H.; Araujo, P. T.; Zhang, X.; Rodriguez-Nieva, J. F.; Lin, Y. X.; Zhang, J.; Kong, J.; Dresselhaus, M. S. Raman Enhancement Effect on Two-Dimensional Layered Materials: Graphene, h-BN and MoS_2. *Nano Lett.* **2014**, *14*, 3033–3040.
38. Zedan, A. F.; Sappal, S.; Moussa, S.; El-Shall, M. S. Ligand-Controlled Microwave Synthesis of Cubic and Hexagonal CdSe Nanocrystals Supported on Graphene. Photoluminescence Quenching by Graphene. *J. Phys. Chem. C* **2010**, *114*, 19920–19927.
39. Tang, W.; Sanville, E.; Henkelman, G. A Grid-Based Bader Analysis Algorithm without Lattice Bias. *J. Phys.: Condens. Matter* **2009**, *21*, 084204.
40. Kresse, G.; Furthmuller, J. Efficiency of *ab-initio* Total Energy Calculations for Metals and Semiconductors Using a Plane-Wave Basis Set. *Comput. Mater. Sci.* **1996**, *6*, 15–50.
41. Grimme, S. Semiempirical GGA-type Density Functional Constructed with a Long Range Dispersion Correction. *J. Comput. Chem.* **2006**, *27*, 1787–1799.